

Seismic Performance of an Actual Member in an Existing RC Building

Mhmoud SAUOD

Graduate Student, Graduate School of Engineering, Hiroshima University

Hideo ARAKI

Professor, Faculty of Engineering, Hiroshima Institute of Technology

Akira YASOJIMA

*Assistant Professor, Graduate School of System and Information Engineering,
Tsukuba University*

Syohei ITANO, Tatsuya TOKUGAWA

Graduate Student, Graduate School of Engineering, Hiroshima University



15 WCEE
LISBOA 2012

SUMMARY:

Studying the seismic performance generally is important step before strengthening buildings which need to be strengthened to resist seismic loads, depending on adequate judgment of structural failure mechanisms because it is one of the most important factors in evaluation of the seismic performance of existing buildings. In Japan, the equation which is used to determine the shear resistance capacity of Reinforced Concrete members was obtained empirically with experimental works in laboratories, but this equation was not checked on real reinforced concrete members individually, so In this research the seismic performance of beams was studied and this equation was checked with studying and comparing the results of experiments using real beam constructed approximately forty years ago and newly constructed beam in the laboratory which designed as close as possible to the real beam, in addition, the seismic performance of an existing beam retrofitted using Epoxy Resin injection and CFRP sheets was studied depending on the results of experimental work of the real beam.

According to the experimental results, a difference in seismic performance between the three beams was obvious. Differences between structural drawings and details of real beam, the influences of deterioration and the effects of retrofitting with warped CFRP sheets and Epoxy Resin injection were discussed based on the test results.

Keywords: Seismic Performance, Actual RC beam, Existing Building, Retrofitting.

1. INTRODUCTION

In Japan, seismic performance of existing buildings has typically been evaluated by seismic diagnosis based on their structural drafts. In many existing buildings however, differences in the strength of materials and arrangement of reinforcement between actual members and the structural drafts have been found. Deteriorations over long duration, uncertainty of construction, scale effects and so on were not considered in the seismic diagnosis of both actual members and specimen manufactured in laboratory. Therefore, it is very difficult to evaluate the accurate seismic performance of an existing building. From this point of view, in the field of civil engineering, performance examinations ^{1), 2), 3)} have been carried out using RC members of an old RC railway bridge, and the applicability of formulas have been evaluated. However, in the field of building engineering, there are very few experimental tests concerning actual RC members of old existing buildings, although full scale experiments have been done using existing buildings ^{4), 5)}. In this paper, actual members were taken out of an existing building constructed approximately forty years ago. The performance of the actual RC members was investigated.

2. SUMMARY OF TESTS

2.1 Existing Building

The target building was a three story reinforced concrete building constructed in 1967, and used as an elementary school building. This building was judged to have a low seismic performance in the seismic diagnosis. The subjected beams located at the end of the slab were removed to reduce story weight and repairing in the retrofitting scheme. The school building is shown in Fig. 1. Elevations of the building are shown in Fig. 2.



Figure 1. Side view of school building

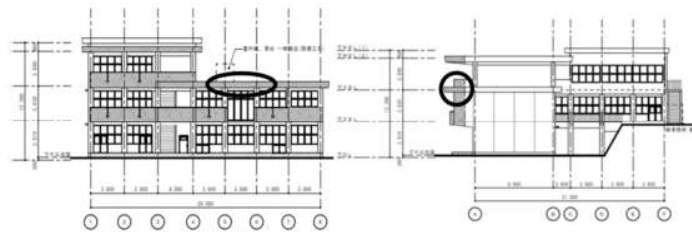


Figure 2. South and East elevations

Table 1. Details of specimens

Specimen	Section $b \times D$ [mm]	Strengthening	Shear Span Ratio M/QD	Main Reinforcement		Shear Reinforcement	
N15	250×450	No	1.5	SS400	2-19 ϕ $p_f=0.5\%$	SS235	2-9 ϕ @300 $p_w=0.17\%$
E15				SR24		SR24	
E15-C1		CFRP + Epoxy					

2.2 Specimens

The actual beams were taken out of the roof slab without any damage using a wire saw. Hoisting of a beam after cutoff is shown in Fig. 3, and two specimens E15 and E15-C1 were prepared. E15 is an existing beam and E15-C1 is the same beam strengthened using CFRP sheets and epoxy resin injection. The number of carbon fiber sheets used was based on the Draft⁽⁶⁾ of Architectural Institute of Japan (2001).

Table 1 shows the properties and specifications of the test specimens including the newly constructed beam. According to the structural draft, main reinforcing for E15 and E15-C1 were round bars 4-19 ϕ (SR24) and transverse reinforcement was round bar 2-9 ϕ (SR24) @300. N15 is a specimen that was manufactured in the laboratory to be as close as possible to the existing beam in terms of dimensions and reinforcement details, where: the main reinforcement was round bar 4-19 ϕ (SS400) and transverse reinforcement was round bar 2-9 ϕ @ 300 (SS235).

The reinforced concrete stubs were manufactured at both ends of the existing beams. The three specimens shared a common shear span length and shear span ratio of 1350 mm and 1.5 respectively. Fig. 4 shows one of the completed existing beams after manufacturing of the stubs. Fig. 5 shows reinforcement details and dimensions of the test specimens. Concrete at both ends was removed to expose longitudinal reinforcement and to allow welding of a steel plate to ensure anchorage before manufacturing stubs for the

existing beams as shown in Fig.6. For the retrofitted existing beam E15-C1, CFRP sheets were used to prevent a brittle shear failure, and epoxy resin was injected along the main bars to prevent slippage of the round reinforcing bars.



Figure 3. Actual beam from the existing building



Figure 4. Completed specimen with stubs

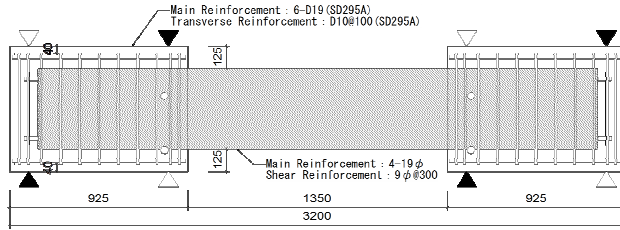


Figure 5. Details of test specimens (reinforcement and dimensions)



Figure 6. Steel plate

2.3 Test Materials

For specimens E15 and E15-C1, compressive strength was obtained by compression tests carried out using twelve concrete cores obtained from both ends of the existing beams. According to the inspection report during seismic diagnosis of this building, the concrete strength of cores from the nonstructural walls was lower than 13.5N/mm^2 (13.5MPa is the recommended lower limit of concrete strength in the Standard for Seismic Evaluation of Existing Reinforced Concrete Building⁷⁾). However, in the compressive tests using cores in this study, compressive strength was not less than 13.5N/mm^2 . The strength was scattered from 13.8N/mm^2 to 22.9N/mm^2 and the average was approximately 18.1N/mm^2 .

The relationship of compressive strength versus modulus of elasticity showed a relatively good correspondence with the formula⁸⁾ as shown in Fig. 7. Where the formula is:

$$E_c = 2.1 \times 10^4 \times (\gamma / 23)^{1.5} \times (F_c / 20)^{1/2} \quad (2.1)$$

E_c : Young's Modulus of Concrete [N/mm^2]

γ : Weight of unit volume of Concrete [kN/m^3]

F_c : concrete compressive strength [N/mm^2]

Tensile tests were performed on the samples from two types of reinforcement 9ϕ and 19ϕ obtained from the building. No major difference was observed although yield strengths were slightly lower than the strengths of reinforcement used in specimen N15. Table 2 and Table 3 show the mechanical properties of concrete and reinforcement of specimens.

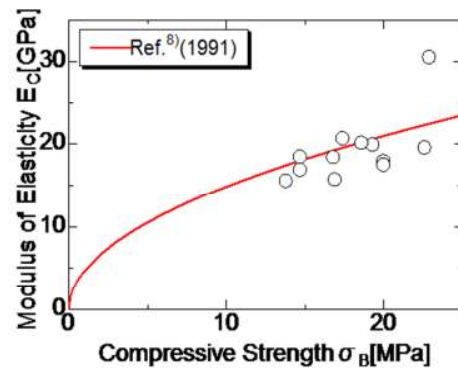


Figure 7. Relationship of compressive strength and Modulus of Elasticity

Table 2. Mechanical properties of concrete

Specimen	Compressive Strength [N/mm ²]	Tensile Strength [N/mm ²]	Modulus of Elasticity [kN/mm ²]	Compressive Strain [μ]
N15	22.3	2.9	22.1	1465
E15 E15-C1	18.1	1.9	19.3	2030

Table 3. Mechanical properties of reinforcement

Specimen		Yield Strength [N/mm ²]	Ultimate Strength [N/mm ²]	Modulus of Elasticity [kN/mm ²]	Yield Strain [μ]
N15	9φ	371.9	494.8	211.5	1885
	19φ	319.0	451.2	202.3	1602
E15 E15-C1	9φ	327.9	425.8	196.2	1885
	19φ	281.3	358.6	201.8	1437

2.4 Loading Procedure

The beams were subjected to reversible loadings by using a universal testing machine with maximum vertical load 100ton and availability to displacement controlling under anti-symmetric moment as shown in Fig. 8.

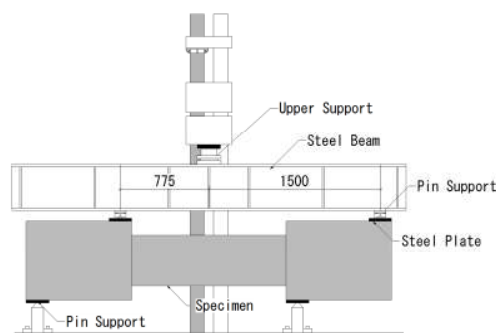


Figure 8. Loading apparatus

The relative shear displacements between the stubs and the local displacements of the beam were obtained using electric displacement transducers instrumented on the rear side of the beam as shown in Fig. 9. The distributions of the flexural and shear deformation were obtained from those data. In specimen N15, strain gauges were attached to main bars to measure strains of these bars

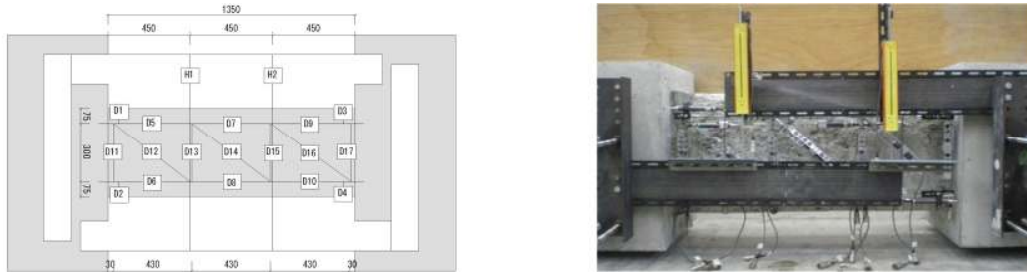


Figure 9. Displacement transducers on the rear side of specimen

3. EXPERIMENTAL RESULTS

3.1 Failure Mode

Fig. 10 shows the failure mode of each specimen. A large difference in failure mechanism between the existing beam E15 and the new one N15 was observed. For new beam N15, flexural cracks had occurred in the boundary surface between both ends of the beam and stubs from $R=1/400\text{rad}$, and their width increased when displacement increased as shown in Fig.10-(a). In addition, a slight shear cracks occurred in the left portion of the beam at drift angle $R=1/400\text{rad}$, but those shear cracks did not progress. The final failure pattern of N15 was bond slippage of the main bars as those bars were plain round bars. On the other hand, for the existing beam E15, flexural cracks occurred at the boundary surface between both ends of the beam and stubs, and shear cracks occurred in the mid area of the beam at drift angle $R=1/400\text{rad}$. With the increasing of deformation, the width of the shear cracks increased when displacement increased. The final failure mechanism was due to shear failure, Large X shaped diagonal cracks were observed as shown in Fig. 10-(b).

For the retrofitted existing beam E15-C1, the flexural cracks were observed at both ends of the beam and it was not possible to observe cracks in the mid area of the beam due to the fiber sheets. After loading, the fiber sheets were removed to inspect the appearance of the mid span of the beam. Disintegration of the concrete cover was observed in the hinging region of the beam.



Figure (10-a) Failure Mode .N15



Figure (10-b) Failure Mode .E15

Cracks in the mid area of the beam body were not observed, as shown in Fig.10-(c). It could not be judged whether the final failure mechanism was bond slip type or flexural failure due to the yielding of the main bars.



Figure (10-c) Failure Mode. E15-C1 after removing fiber

3.2 Relationship of Shear strength and Drift Angle

Fig. 11 shows the relationship of shear strength versus drift angle. The strength of specimen N15 reached maximum strength at drift angle $R=1/200$ rad. The peak of the shear strength of each loading cycle did not decrease very rapidly. From the shape of the hysteresis loops it is found that bond slip of the main bars had an influence on the restoring force characteristics. Although the critical drift angle was approximately $R=1/32$ rad. The stiffness near the origin was very low due to the bond deteriorations when the displacement increased. For specimen E15, the strength had reached maximum strength at drift angle $R=1/200$ rad.

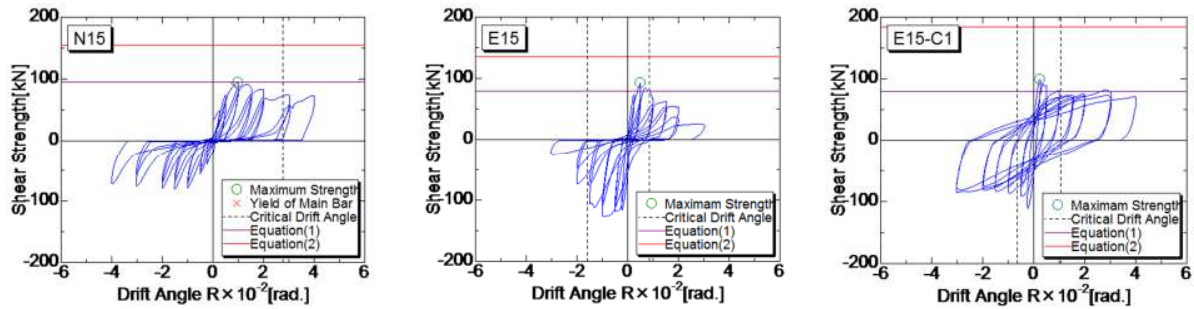


Figure 11. Relationship of shear force versus drift angle

After the maximum strength was reached, the strength decreased rapidly. The hysteresis loops show a pinched shape in the vicinity of the origin. The critical drift angle was $R=1/100$ rad, which was less than that for N15. For specimen E15-C1 the strength had reached maximum value at drift angle $R=1/400$ rad in the first loading cycle. After the strength slightly decreased, it then became constant. The main bars had yielded according to the shape of the shear force loops which were a spindle type. Calculated values of flexural strength and shear strength using the following equations⁷⁾ are shown in the Figure. It was assumed that the bars arrangement were the same as in the structural drafts. Material strengths were obtained in the material tests performed before the loading tests. The strength was substantially greater than the value obtained by the flexural formula Eqn. (3.1).

$$M_u = 0.9 \cdot a_t \cdot \sigma_y \cdot d \quad (3.1)$$

M_u : moment strength [kNm]

a_t : area of main reinforcement [mm^2]

σ_y : yield strength of main reinforcement [N/mm^2]

d : effective depth of beam [mm]

$$Q_{su} = \left\{ \frac{0.053p_t^{0.23}(18+F_c)}{M/(Q \cdot D) + 0.12} + 0.85\sqrt{p_w \cdot \sigma_{wy}} \right\} b \cdot j \quad (3.2)$$

Q_{su} : shear strength [kN]

p_t : tensile reinforcement ratio [%]

F_c : concrete compressive strength [N/mm²]

$M/(QD)$: shear span ratio.

p_w : shear reinforcement ratio.

σ_{wy} : yield strength of shear reinforcement [N/mm²]

b : beam width [mm]

j : distance between centers of stresses ($7/8d$) [mm]

The strength of each specimen was close to the value calculated by Eqn. (3.1). The critical drift angle was $R=1/100$ rad. For specimen E15, the calculated shear strength by Eqn. (3.2) was much greater than the observed strength although the failure mode of this specimen was shear failure.

3.3 Energy Absorption Capacity

Fig. 12 shows the amount of energy absorption of each specimen. There was a slight difference in the increasing of energy absorption between N15 and E15, but there was an obvious difference between these specimens and the retrofitted specimen E15-C1, as can be seen in Fig. 12. For N15, increasing of energy absorption was approximately linear until the final failure with maximum value of approximately 10kN·m at drift angle $R=1/25$ rad. The same properties were observed in E15, but when the deformation increased over drift angle $R=1/50$ rad, the energy absorption was close to being constant. On the other hand, in the retrofitted beam E15-C1, the energy absorption was the same as the other two specimens before $R=1/100$ rad, and then began to increase rapidly. The rapid increase of E15-C1 resulted from yielding of the main bars. The energy absorption eventually neared 25kN·m, which was 2~3 times of those of the beams without retrofitting.

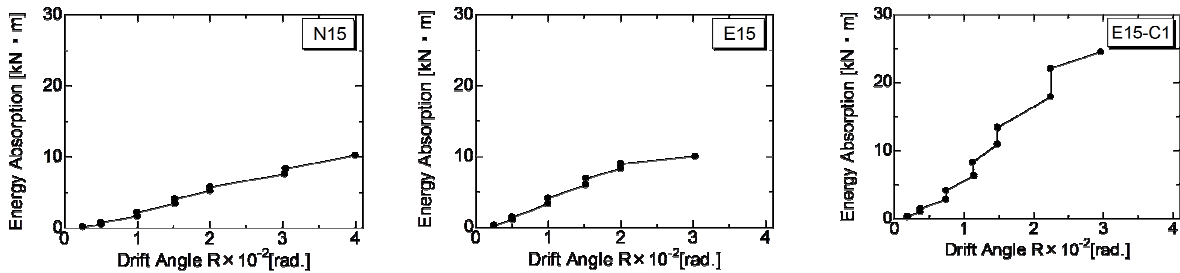


Figure 12. Energy Absorption

3.4 Flexural Deformation Rate

Fig. 13 shows the relationship of drift angle versus percentage of flexural deflection. The flexural deflection was obtained by subtracting the shear deflection from total deflection. Shear deflection was obtained by the local displacement measured with displacement transducers as shown in Fig. 9. For the retrofitted beam E15-C1, the initial state of flexural deflection accounted for 80% to 90% of the total, similar to the other specimens. This flexural deflection was due to bond slip of the main bars or main bars yielding, because most of the flexural cracks were observed at both of the beam ends. For specimen E15, the initial percentage of flexural deformation was about 80% and then decreased rapidly because of

the brittle shear failure, with final percentage of shear deformation at about 70%.

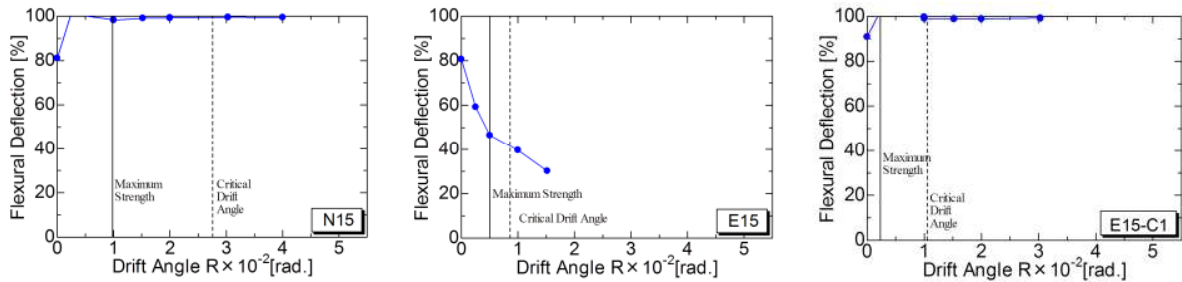


Figure 13. Percentage of flexural deformation to total deformation

4. DISCUSSIONS

4.1 Characteristics of Shear Force Envelopes

Fig.14 shows the envelopes of the three specimens' restoring characteristics. There was an obvious difference between these envelopes. For specimen N15, differences in the positive and negative directions of loadings were observed. These differences are a result of the occurrence of the bond slip and the positive loading affect on the restoring force characteristic in the negative loadings. For both specimens E15 and E15-C1, envelope curves were almost the same in the positive and negative directions. For E15-C1, envelope was stable in both positive and negative directions.

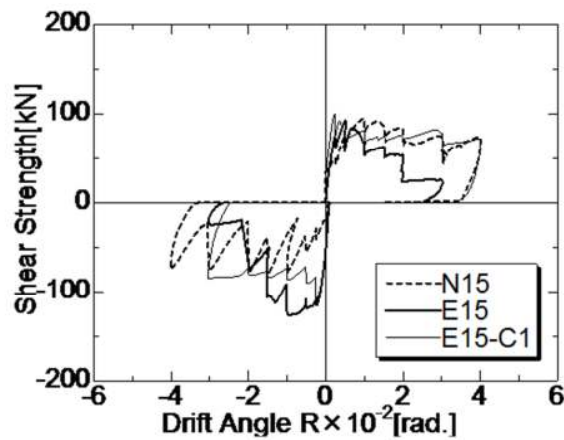


Figure 14. Envelope Curves of shear force-drift angle

4.2 Maximum Strength

Table 4 shows the observed and calculated maximum strength. The calculated flexural and shear values were obtained using Eqn. (3.1) and Eqn. (3.2). The material strength from the material tests were used in the calculations. Because yielding of the main bars was observed in the specimen N15 regardless of bond slip failure the observed maximum strength was close to that calculated.

Table 4. Maximum strength

Specimen	Observed [kN]	Flexural		Shear	
		Calculated [kN]	Observed/ Calculated	Calculated [kN]	Observed/ Calculated
N15	94.3	94.4	1.00	154.1	0.61
E15	92.4	83.3	1.11	137.5	0.67
E15-C1	99.0	83.3	1.19	184.2	0.54

For specimen E15, the maximum strength was greater than the calculated flexural strength by approximately 1.11 times and less than the calculated shear strength by approximately 0.67 times. It was found for the existing beam that the maximum strength based on the failure mechanism could not be predicted. For retrofitted beam E15-C1, the maximum strength was greater than the calculated flexural strength by approximately 1.2 times. For specimen E15, after loading, the concrete cover was removed to reveal more information about reinforcement details as shown in Fig. 15~17. In the structural drafts, intervals of the stirrups were 300mm, but in the actual beam, intervals were approximately 500mm with 90 degree hooks at the connection to the main bars. The additional length at the hook was 40mm.

Because round bars were used for the stirrups, it is a possibility that a stirrup fell out of the concrete. Therefore, the stirrups were not effective in preventing shear cracks. In addition, the actual beam depth D was greater than 500mm, but $D=450$ mm in the structural drafts. The difference in depth between the structural draft specifications and the actual cross-section would have an effect on the shear span ratio (M/QD) and relative shear reinforcement ratio p_w . The cross-section shape of the existing beam was a

Table 5. Maximum strength values with consideration of actual cross-section details

Specimen	Observed [kN]	Flexural		Shear	
		Calculated [kN]	Observed/ Calculated	Calculated [kN]	Observed/ Calculated
E15	92.4	92.9	0.99	94.9	0.97

parallelogram rather than a rectangle. Based on the details of the actual beam the analysis was performed again assuming a stress block. The results of the analysis are shown in Table 5. The calculated shear strength became closer to the maximum of approximately 0.97. The calculated shear strength was not lower than the calculated flexural strength, although the final failure mechanism was a brittle shear failure. From the Design Guidelines of AIJ⁹⁾ the calculated shear cracking strength was approximately 80.2kN, and the maximum shear strength was 105.2kN. Further inspection is required to predict the maximum strength of the existing RC members.



Top side



Bottom side

**Figure 16.** Stirrups with 90° hook**Figure 15.** Main reinforcement at beam ends

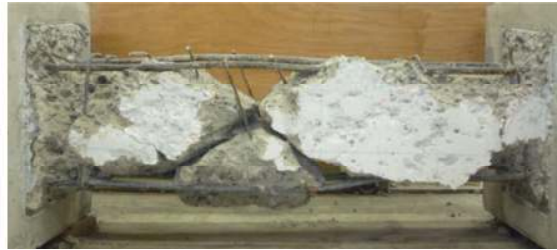


Figure 17. Bars arrangement

5. CONCLUSIONS

Based on the experimental results the following conclusions were made;

- 1) According to structural drafts, the failure mechanism was expected to be flexural failure, but failure patterns were shear failure of the existing beam and bond slip failure for the newly constructed beam.
- 2) There were obvious differences in the existing beam cross-section when comparing the actual section and structural drafts, particularly section shape and reinforcement details. In addition, construction precision has a great effect on the maximum strength.
- 3) The maximum strength of existing beams can be approximately estimated by examining the cross-sectional properties.
- 4) The seismic performance of the retrofitted RC beams using epoxy and CFRP sheets was significantly improved.

ACKNOWLEDGEMENTS

This research has been supported by the Japan Ministry of Education, Culture, Sports, Science and Technology under Grant-in-aid No.21360268. The authors would like to thank the staff and graduate students of the Structural Earthquake Engineering Laboratory of Hiroshima University.

REFERENCES

- 1) Yokozawa et al. (2005). Degradation and Structural Performance of RC pier super structure in service. *Conference on Structural Engineering and Construction*. Vol 27: 2.
- 2) Niitani et al. (2005). Studies on loading and durability of prestressed concrete member which was in service for 38 years. *Pacific Conference on Structural Engineering and Construction*. Vol 27:2: 1585-1590.
- 3) Hattori et al. (2006). Mechanical Properties of RC railway member has been in service for 60 years. *Pacific Conference on Structural Engineering and Construction*. Vol 28:2:1621-1626.
- 4) Yutaka Osawa, Hiroyuki Aoyama, Isao Funahashi. (1968). Destruction of the old building vibration and Tokyo Marine Bill Part (2)-Examination of safety against seismic force. *Concrete Journal*. Vol 6: 6:16-26.
- 5) Yutaka Matsushima. (1970). The experimental tests reported of full scale destruction of the reinforced concrete wall-type five-storey apartment. *Concrete Journal*. Vol 8:1:11 - 21.
- 6) Architectural Institute of Japan. (2001), the Draft of Design and Construction of Continuous Fiber Reinforced Concrete Structural System, Architectural Institute of Japan.
- 7) Japan Building Disaster Prevention Association. (2001), Standards of seismic diagnosis of existing RC buildings, Japan Building Disaster Prevention Association.
- 8) Architectural Institute of Japan. (1991), Standard Calculation of Reinforced Concrete Structure, Architectural Institute of Japan.
- 9) Architectural Institute of Japan. (1997), Design Guidelines for Earthquake Resistant Reinforced Concrete Buildings Based on inelastic Displacement Concept, Architectural Institute of Japan.